

# System identification of the suspension tower of Runyang Bridge based on ambient vibration tests

Zhijun Li<sup>\*1</sup>, Dongming Feng<sup>2a</sup>, Maria Q. Feng<sup>3b</sup> and Xiuli Xu<sup>1c</sup>

<sup>1</sup>College of Civil Engineering, Nanjing Tech University, Nanjing, 211800, China

<sup>2</sup>Weidlinger Transportation Practice, Thornton Tomasetti, New York, NY 10005, USA

<sup>3</sup>Department of Civil Engineering and Engineering Mechanics, Columbia University, New York, NY 10027, USA

(Received October 23, 2016, Revised January 20, 2017, Accepted January 27, 2017)

**Abstract.** A series of field vibration tests are conducted on the Runyang Suspension Bridge during both the construction and operational stages. The purpose of this study is devoted to the analysis of the dynamic characteristics of the suspension tower. After the tower was erected, an array of accelerometers was deployed to study the evolution of its modal parameters during the construction process. Dynamic tests were first performed under the freestanding tower condition and then under the tower-cable condition after the superstructure was installed. Based on the identified modal parameters, the effect of the pile-soil-structure interaction on dynamic characteristics of the suspension tower is investigated. Moreover, the stiffness of the pile foundation is successfully identified using a probabilistic finite model updating method. Furthermore, challenges of identifying the dynamic properties of the tower from the coupled responses of the tower-cable system are discussed in detail. It's found that compared with the identified results from the freestanding tower, the longitudinal and torsional natural frequencies of the tower in the tower-cable system have changed significantly, while the lateral mode frequencies change slightly. The identified modal results from measurements by the structural health monitoring system further confirmed that the vibrations of the bridge subsystems (i.e., the tower, the suspended deck and the main cable) are strongly coupled with one another.

**Keywords:** system identification; suspension bridge tower; ambient vibration test; pile-soil-structure interaction; tower-cable system; structural health monitoring system

## 1. Introduction

Recently, advanced sensor technologies together with efficient time- and frequency-domain identification techniques have been developed and utilized for structural health monitoring (SHM), including modal identification, finite element (FE) model updating and damage detection, etc. (Brownjohn, Moyo *et al.* 2005, Li, Ou *et al.* 2006, Feng and Feng 2015, Feng, Feng *et al.* 2015, Feng, Sun *et al.* 2015, Ni, Wang *et al.* 2015). Performances of long-span bridges (e.g., suspension bridges) subjected to external excitations depend largely on the structural dynamic properties. Although these properties can be modeled using sophisticated analytic models, real behaviors of large-scale structures remain to be verified from field vibration tests (Rice, Mechitov *et al.* 2010, Li, Laima *et al.* 2011). During the past two decades, efforts have been made to study characteristics of suspension bridges based on either short-

term or long-term measured data from SHM systems (Abdel-Ghaffar and Scanlan 1985, Ren, Harik *et al.* 2004, Gentile and Gallino 2008, Li 2010, Deng, Liu *et al.* 2015).

The tower substructure represents one of the most critical components of a suspension bridge, which is extremely susceptible to vibrate under wind and seismic excitations (Siringoringo and Fujino 2012). Although considerable full-scale field tests have been conducted on suspension bridges (Ko, Xue *et al.* 1998), due to reasons such as inaccessibility, there are fewer studies focusing on tower vibrations (Feng, Kim *et al.* 1998). Moreover, there have been little reported studies investigating the evolution of tower modes from its freestanding condition to tower-cable condition during construction. Besides, despite the advances in the FE modeling and system identification, tower-foundation-pile interactions are not often accurately accounted for due to the inherent uncertainties in defining the dynamic stiffness and associated computational difficulty (Sun and Bueyuekoeztuerk 2016, Sun, Mordret *et al.* 2017). The most reliable method is to study the structure-soil-foundation system as a whole. However, the majority of current studies focus on laboratory testing of scaled soil-structure models, tested either on a shaking table or in a centrifuge, with controlled soil conditions and subject to inevitable limitations of scaling (Zhang, Prader *et al.* 2012).

On the other hand, challenges would arise when identifying the modal properties of the tower substructure from responses of the tower-cable system. Since dynamic

\*Corresponding author, Associate Professor

E-mail: [lizhijun@njtech.edu.cn](mailto:lizhijun@njtech.edu.cn)

<sup>a</sup> Ph.D.

E-mail: [df2465@columbia.edu](mailto:df2465@columbia.edu)

<sup>b</sup> Professor

E-mail: [mqf2101@columbia.edu](mailto:mqf2101@columbia.edu)

<sup>c</sup> Professor

E-mail: [njxuxiuli@163.com](mailto:njxuxiuli@163.com)

properties of a freestanding tower are different from those based on tower-cable system analysis. One major challenge is how to distinguish the “true” natural frequencies and mode shapes of the tower as a sub-component of the coupled global structure from the pool of possible candidates. In fact, to conduct reliable modal identification, the dynamic behavior and interactions of the global system and individual sub-components must be clearly conceptualized. The purpose of this study is devoted to the analysis of the life-cycle dynamic characteristics of the suspension tower. Based on the identified modal parameters, the effect of the pile-soil-structure interaction on dynamic characteristics of the suspension tower is investigated. Moreover, the stiffness of the pile foundation is successfully identified using a probabilistic finite model updating method.

The paper is organized as follows: In Section 2, descriptions of the suspension bridge and the ambient vibration tests are introduced. In Section 3, field test results of the freestanding tower are presented, and dynamic properties of the freestanding tower are identified based on the ambient fields test. In Section 4, challenges of identifying tower dynamic properties from the response of a tower-cable system are studied by comparing the identified results between those from the freestanding tower and the tower-cable system. In Section 5, a FE model of the tower considering the pile-soil-tower interaction has been developed, from which the probabilistic-based method is adopted to identify the stiffness of the pile foundation. Moreover, a 3D global FE model of the bridge is developed to accurately reproduce the identified modal properties from measured responses. Section 6 concludes this work.

## 2. Description of Runyang Suspension Bridge and ambient field tests

### 2.1 Bridge description

The Runyang Suspension Bridge (RYSB), as shown in Fig. 1, is one of the most critical traffic links spanning the Yangtze River, China. At the time of its completion in 2005, it was the longest suspension bridge in China. RYSB consists of a 1490 m main span and two 470 m side spans. The steel orthotropic box girder deck has a width of 36.3 m. The main cable is composed of parallel subsection cables. The main span is supported by two towers, each approximately 210 m tall. Each of the two concrete towers (the south tower in Zhenjiang side and the north tower in Yangzhou side) is composed of two reinforced concrete columns connected by three horizontal prestressed cross-beams at different levels. The tower is founded on 8×4 rows of piles, each of which has a diameter of 2.8 m and length of 60m, as shown in Fig. 2.

### 2.2 Field ambient vibration tests

Since the erection of the tower, a series of ambient vibration tests were conducted on the freestanding tower with a purpose of studying the evolution of its modal

parameters during the construction process. The first test was performed on the freestanding tower in 2002 before the main cable being installed. The second test was conducted on the tower-cable system in December 2004 when the construction of the suspension bridge was completed.

Tower responses are measured at various locations using high-sensitivity accelerometers. As illustrated in Figs. 3 and 4, there are a total of 11 measurement points. The tower responses of the longitudinal component are firstly recorded for more than half an hour. Then, the sensors were turned 90 degrees to measure the lateral responses. Signals from accelerometers are amplified and filtered. The sampling frequency in the field tests is 20Hz. In this study, frequencies higher than 10Hz are filtered out from the tower measurements.

In addition, during the second test of the tower-cable system, a full-scale test of the main deck was also conducted to identify the main-span dynamic properties based on a dense set of sensor placement along the bridge deck. As illustrated in Fig. 5, a total of 45 vibration stations/sections are arranged on the structure. At each measurement station, two vertical (both at upstream and downstream sides) and one lateral components of the vibration response are recorded. Of these 45 stations, two sensors were maintained fixed at a reference section located close to one third of the central span (position 18 in Fig. 5), whereas the other two sensors roved all the other upstream/downstream measurement points.



Fig. 1 View of the Runyang Suspension Bridge

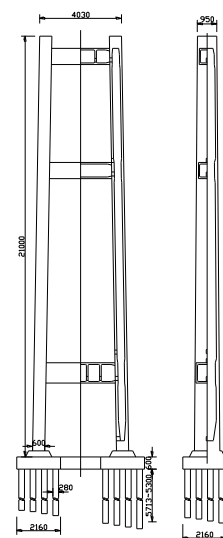


Fig. 2 View of the Runyang Suspension Bridge Tower (Unit:cm)



Fig. 3 View of the bridge tower

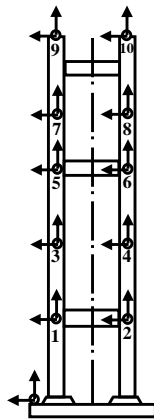


Fig. 4 Layout of the tower measurements

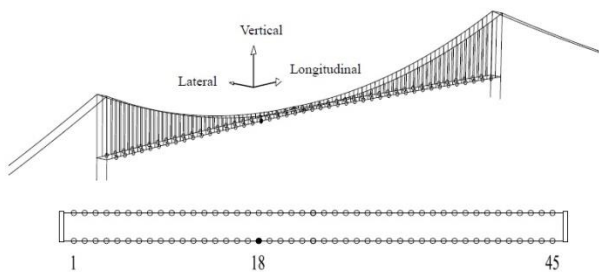


Fig. 5 Measurement points used in ambient vibration test of the girder

### 2.3 System identification method

When a large-scale structure is subjected to natural and man-made excitation such as wind, traffic, and water waves or their combinations, it is extremely difficult to measure the input dynamic forces acting on the structure. Thus, only the structural responses are measured. Ambient vibration data is conventionally processed using the peak picking (PP) approach to obtain the frequency-domain information. During past three decades, there have been some advanced modal parameter identification methods to choose from, especially for cases of output-only modal analysis, such as eigensystem realization algorithm (ERA), stochastic

subspace identification (SSI) (Ulusoy and Feng 2011, Van Overschee and De Moor 2012) and enhanced frequency domain decomposition (EFDD), etc. (Rune, Lingmi *et al.* 2001). The EFDD method is a more advanced frequency method, which consists of computing the singular value decomposition (SVD) of the spectrum matrix. In some sense, the EFDD method can be considered as an SVD extension of the PP method. Since SVD has the ability of separating signal space from noise space, the closely spaced modes can easily be identified.

Considering that the modes of the tower are well separated, the classical identification technique that use spectra analysis was adopted to identify the modal parameters of the tower. The initial identification of the tower frequencies and mode shapes was conducted using the PP approach and the EFDD technology. One of the major advantages of the method is its speed: the identification can be done on-line allowing a quality check of the acquired data on site. Operational deflection shapes (ODSs) were computed for each frequency corresponding to an identified peak using the magnitude and phase information from the cross-power spectra for output pairs from responses at each measurement level and the selected reference level on the towers. The phase information between each output pair was whitewashed to force normal mode characteristics on the ODSs.

## 3. Dynamic analysis of the freestanding tower

### 3.1 Field test result of the freestanding tower

The power spectral density (PSD) of a typical longitudinal response measured from the freestanding tower is plotted in Fig. 6. Most of the frequencies are well separated. There are 9 modes identified for the tower in the frequency range of 0~3.5 Hz.

Figs.7 through 9 are respectively the longitudinal, lateral and torsional mode shapes of the freestanding tower. Meantime, a finite element model is developed with beam elements. To simplify the simulation of the pile foundation, a fixed boundary condition was assumed.

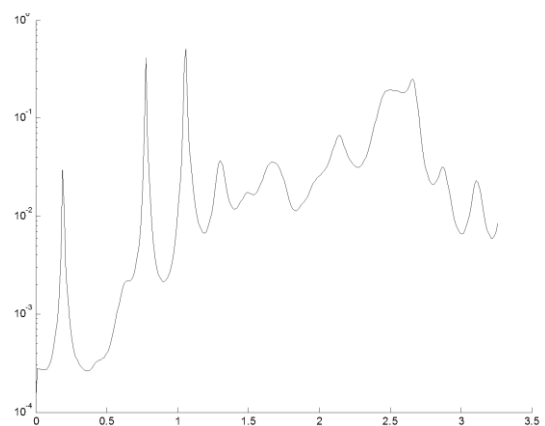


Fig. 6 PSD of the response of the freestanding tower

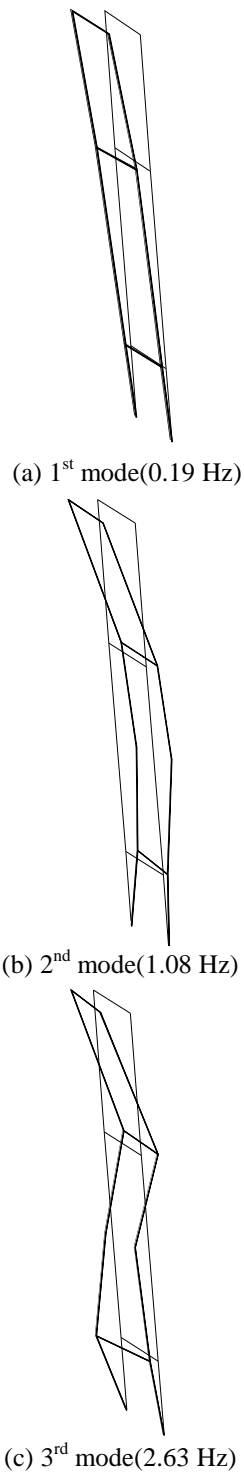


Fig. 7 Measured longitudinal modal shapes of the freestanding tower

Figs. 10 through 12 plot the simulated modal shapes. The comparison between the measured mode shapes and calculated ones demonstrates a satisfactory agreement. Table 1 compares the measured and simulated modal frequencies of the freestanding tower. It can be observed that most of the calculated results give relatively higher values, which probably due to the ignorance of pile-soil-structure interaction.

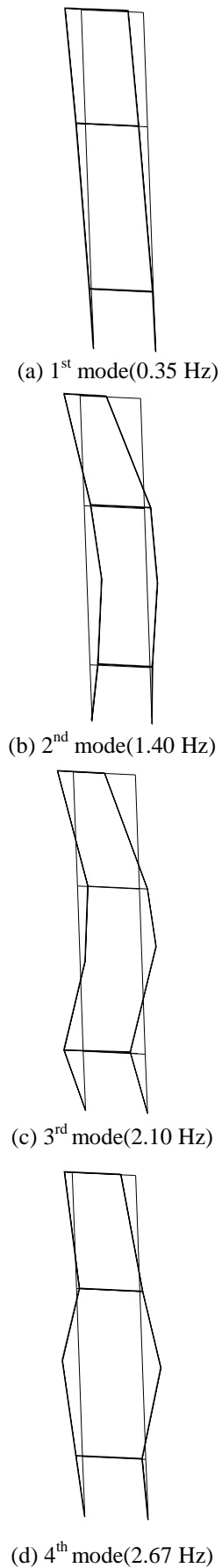


Fig. 8 Measured lateral modal shapes of the freestanding tower

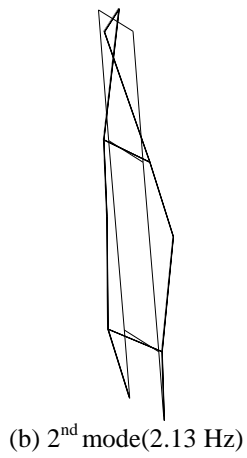
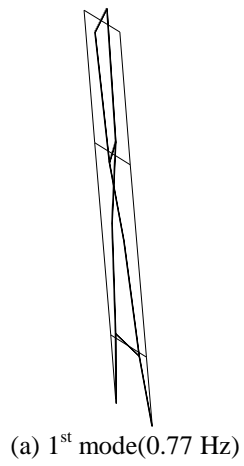


Fig. 9 Measured torsional modal shapes of the freestanding tower

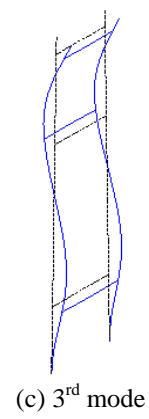
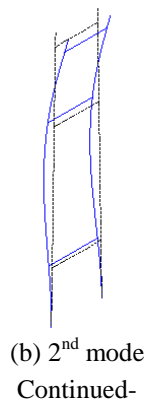
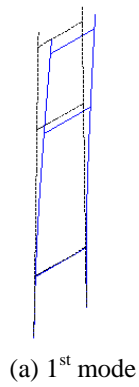
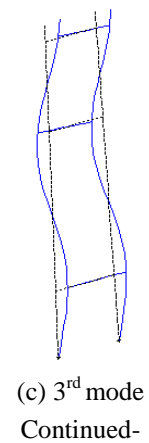
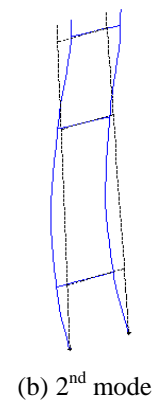
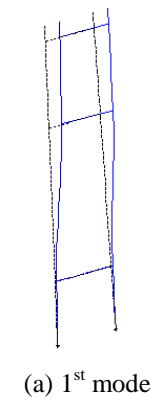


Fig. 10 Calculated longitudinal modal shapes of the freestanding tower



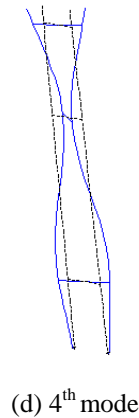
(d) 4<sup>th</sup> mode

Fig. 11 Calculated lateral modal shapes of the freestanding tower

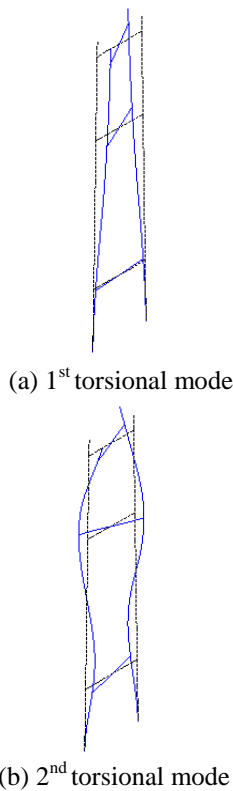
(a) 1<sup>st</sup> torsional mode(b) 2<sup>nd</sup> torsional mode

Fig. 12 Calculated torsional modal shapes of the freestanding tower

## 4. Dynamic analysis of the tower-cable system

### 4.1 Analysis of the field tests of the tower-cable system

To study the evolution of the tower modal parameters during the construction process, tests were carried out using the tower sensors in Fig. 4 after the main cable, hangers and main girder are installed, as shown in Fig. 1. To investigate the coupled effects among the bridge subsystems, measurements of the main girder were also made using the sensor deployment in Fig. 5.

Table 1 Measured and calculated dynamic properties of the freestanding tower

Mode number	Symbol	Frequencies (Hz)		Relative discrepancy (%)	Modal shapes
		Measured	FE model		
1	L1	0.192	0.198	3.1	1st longitudinal bending mode
2	L2	1.080	1.067	-1.2	2nd longitudinal bending mode
3	L3	2.630	2.670	1.5	3rd longitudinal bending mode
4	LL1	0.350	0.359	2.6	1st lateral bending mode
5	LL2	1.400	1.445	3.2	2nd lateral bending mode
6	LL3	2.100	2.135	1.7	3rd lateral bending mode
7	LL4	2.670	2.591	-3.0	4th lateral bending mode
8	T1	0.770	0.828	7.5	1st torsional mode
9	T2	2.130	2.205	3.5	2nd torsional mode

#### 4.1.1 Longitudinal tower modes

Fig. 13 plots the PSDs of the longitudinal responses of the tower from the ten tower sensors in Fig. 4. The first four longitudinal mode shapes are plotted in Fig. 14. Note that the mode shapes with frequencies of 0.54 Hz and 0.60 Hz are associated with the vertical vibration of the suspended structure, which are not available in the freestanding tower. The 1<sup>st</sup> and 2<sup>nd</sup> purely longitudinal tower modes are denoted as mode L1 (0.68 Hz) and mode L2 (1.52 Hz).

Fig. 13 also shows a few obvious resonant frequencies at 0.122 Hz, 0.144 Hz, 0.169 Hz, 0.240 Hz, and 0.276 Hz, which are frequencies of the global tower-cable system.

This can be confirmed by analyzing the vertical responses measured by girder sensors in Fig. 5. Fig. 15 shows the PSDs of vertical responses obtained at point 61 and 89 on the girder, respectively. Fig. 16 plots the first four identified mode shapes of the main-span girder identified from the deployed girder sensors, i.e., 1<sup>st</sup> vertical bending mode, 1<sup>st</sup> anti-symmetric vertical mode, 2<sup>nd</sup> vertical symmetric mode and 1<sup>st</sup> symmetric torsional mode, and these mode shapes are compared with those from FE models (later described in Section 5.4). Therefore, it is concluded that some of the resonant frequencies of the tower are incidental to the ones of the main-span girder, meaning that the longitudinally coupled vibrations between the tower and suspended structure.

#### 4.1.2 Lateral tower modes

Fig. 17 shows the PSDs of lateral responses of the tower from five tower sensors. Note that the first two obvious frequencies at 0.232 Hz and 0.256 Hz are incidental to the cable vibrations. The most dominant frequency is around 0.35 Hz, which is the 1<sup>st</sup> lateral mode.

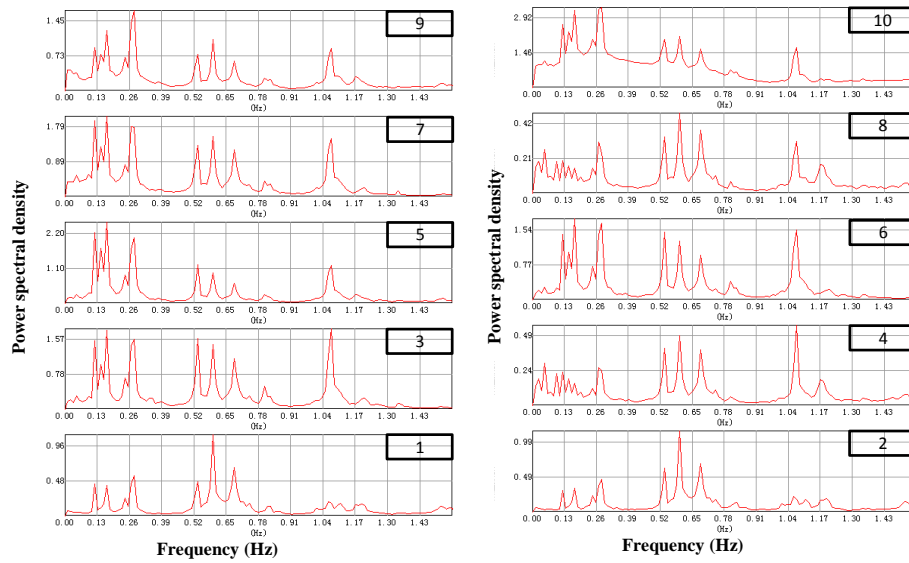


Fig. 13 PSDs of longitudinal responses of the tower in the tower-cable system

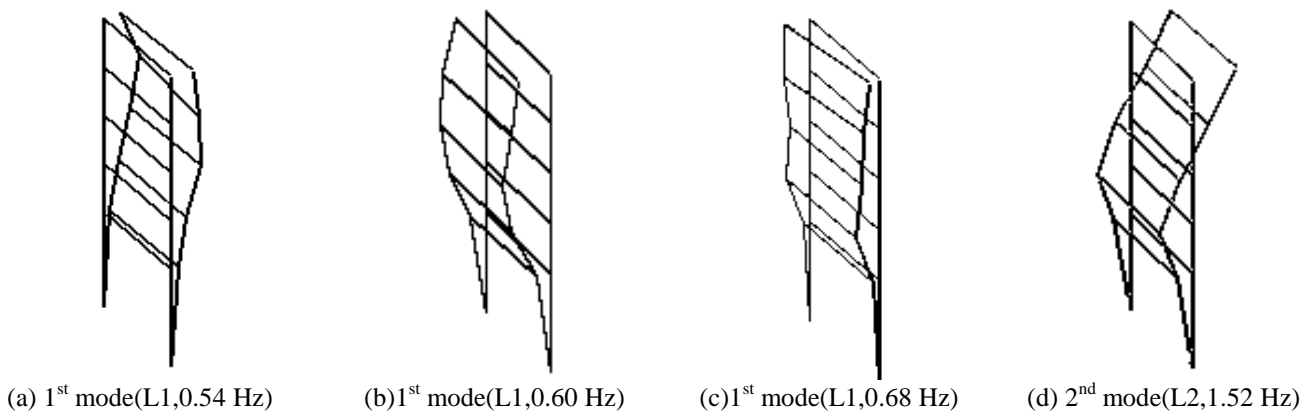


Fig. 14 Identified longitudinal mode shapes of the tower in the tower-cable system

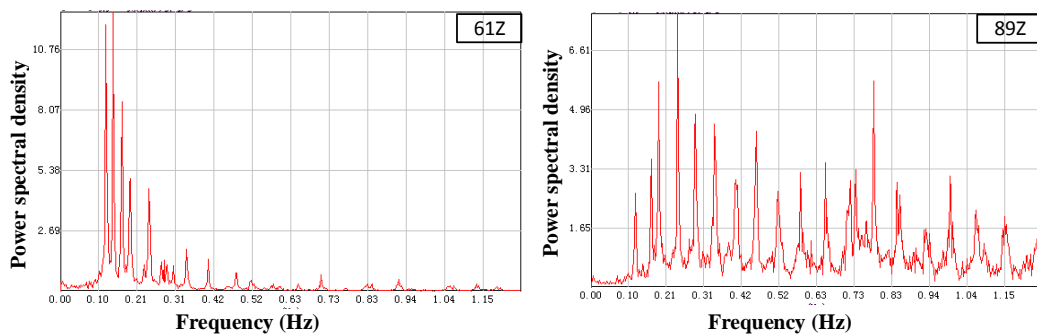
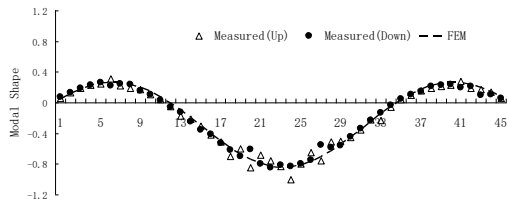


Fig. 15 PSD of the vertical responses at deck points 61 and 89

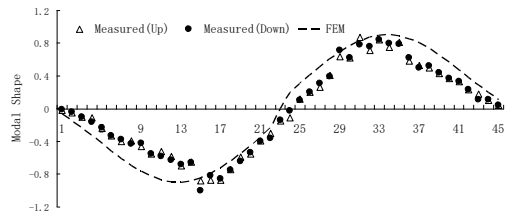
The next distinct frequency peak at 0.391 Hz is also associated with the cable vibration. The 2<sup>nd</sup> and 3<sup>rd</sup> lateral tower mode is marked as mode LL2 (1.42 Hz) and mode LL3 (2.17 Hz) in Fig. 18.

It's also noted that the PSDs of the identified lateral frequencies of the tower in Fig.17 include several cable

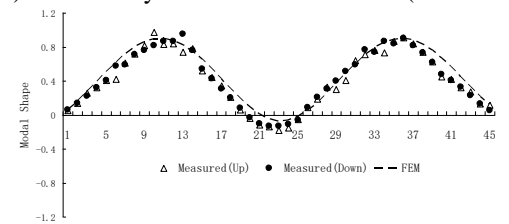
frequencies, meaning a strong lateral coupled vibration between the tower and the main cable. Since there are no girder frequencies available in Fig.17, there would be no or weak lateral coupled vibrations between the tower and the bridge deck.



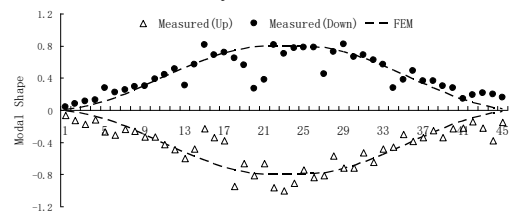
(a) First vertical bending mode (0.122 Hz)



(b) First anti-symmetric vertical mode (0.144 Hz)



(c) Second vertical symmetric mode (0.169 Hz)



(d) First symmetric torsional mode (0.240 Hz)

Fig. 16 Identified vertical modal shapes of the main-span girder

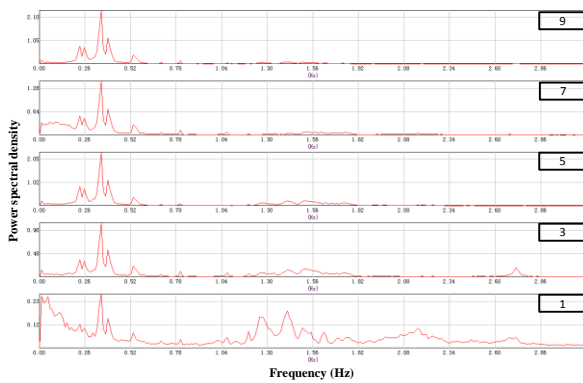
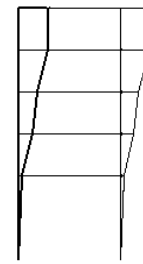


Fig. 17 PSDs of lateral responses of the tower in the tower-cable system

4.1.3 Torsional tower modes

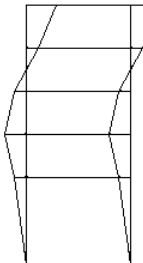
The first three identified torsional mode shapes (T1, T2 and T3) of the tower are shown in Fig. 19, corresponding to natural frequencies of 1.07 Hz, 2.42 Hz and 3.49 Hz, respectively. Note that analysis shows mode T3 are associated with the torsional vibrations of the suspended structure.



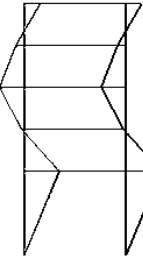
(a) LL1 mode (0.35 Hz)



(b) LL2 mode (1.42 Hz)



(c) LL2 mode (1.51 Hz)



(d) LL3 mode (2.17 Hz)

Fig. 18 Identified lateral modal shapes of the tower in the tower-cable system



(a) 1st torsional mode (T1, 1.07 Hz)

Continued-

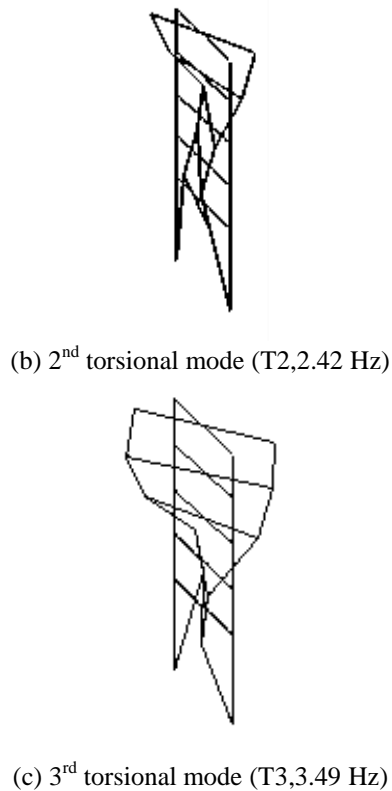


Fig. 19 Identified torsional modal shapes of the tower in the tower-cable system

#### 4.2 Results comparison between the freestanding tower and tower in the tower-cable system

Table 2 tabulates the frequencies identified from the freestanding tower and tower in the tower-cable system. Comparing to the freestanding tower, the tower frequencies of the longitudinal and torsional modes in the tower-cable system have significantly changed, while the frequencies in the lateral direction change slightly. Moreover, the installation of the cable system and erection of main girder result in a much more complex tower dynamic characteristics, due to the coupled vibrations incidental to those of the main girder and main cable.

#### 4.3 Vibration analysis of the tower-cable system using the SHM system

As discussed above, the tower-cable system exhibits strong coupled characteristics. To confirm the findings, the vibration measurements obtained from the SHM system of the RYSB during the operational stage are analyzed.

After the completion of the RYSB in 2005, a permanent SHM system was installed and has been conducting real-time bridge response measurement. The accelerometer layout of the SHM system is shown in Fig. 20, with 8 lateral accelerometers and 4 vertical accelerometers on the four sections of the main cable, 29 accelerometers on the nine sections of the main-span bridge deck, and 12 accelerometers installed on the north and south tower, respectively. Thus, there are a total of 65 accelerometers.

Table 2 Measured dynamic properties of the tower-cable system

	Frequencies (Hz)		Relative Change (%)	Modal shapes	
	Tower-cable system	Freestanding tower			
Longitudinal	L1	0.54	---	---	Associated with bridge vertical vibration
	L2	0.60	---	---	Associated with bridge vertical vibration
	L3	0.68	0.19	70.6	1st longitudinal bending mode
	L4	1.52	1.08	28.9	2nd longitudinal bending mode
Lateral	LL1	0.35	0.35	0.0	1st lateral bending mode
	LL2	1.42	1.40	1.4	2nd lateral bending mode
	LL3	1.51	---	---	Associated with bridge lateral vibration
	LL4	2.17	2.13	1.8	3rd lateral bending mode
Torsional	T1	1.07	0.77	28.0	1st torsional mode
	T2	2.17	---	---	Associated with bridge vertical vibration
	T2	2.42	2.13	12.0	2nd torsional mode
	T2	3.49	---	---	3rd torsional mode

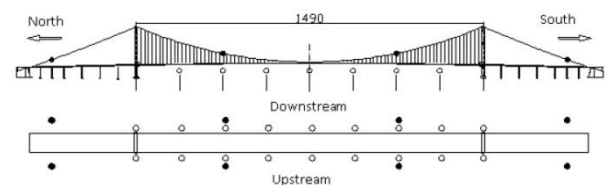


Fig. 20 Layout of accelerometers in SHM system of the RYSB

Fig.21 plots one of the PSDs of the longitudinal responses recorded from the South Tower, while Fig. 22 plots one of the PSDs of the vertical responses of the main-span deck. It can be seen that the measured longitudinal mode frequencies of the tower include several frequencies of the suspended structure. Figs. 23 and 24 respectively plot one of the PSDs of the lateral responses of the main cable and one of the PSDs of the lateral responses of the main-span deck, showing that deck lateral frequencies also include several cable frequencies. By comparing the modal results identified from the tower, the suspended deck and the main cable, it's confirmed that the vibrations of the bridge subsystems are strongly coupled with one another.

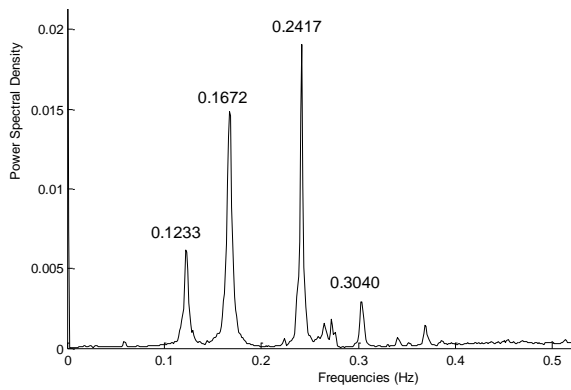


Fig. 21 PSD of longitudinal response of the South Tower

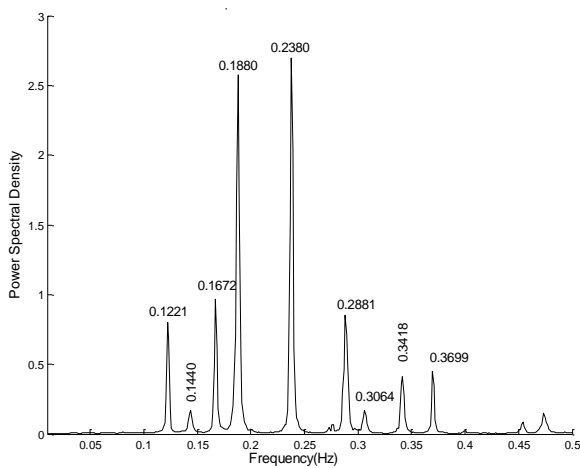


Fig. 22 PSD of vertical response of the central span girder

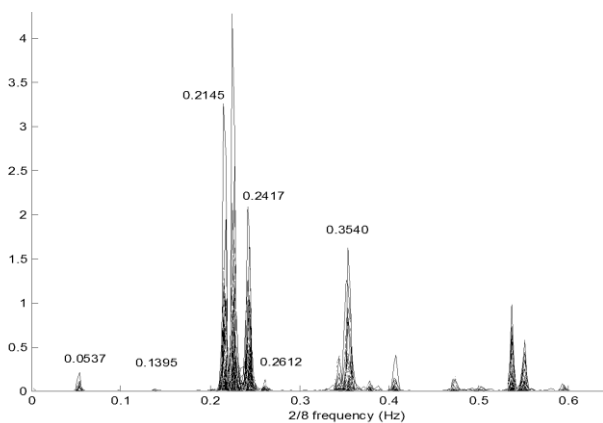


Fig. 23 PSD of the lateral response of the main cable

## 5. FE model update of the freestanding tower and the tower-cable system

### 5.1 3D Solid FE modeling of the freestanding tower

To account for the effect of the pile-soil-structure interaction on the tower dynamic properties, a 3D FE model

of the tower is developed. The soil and pile are modeled in the FE model using software ANSYS, as illustrated in Fig. 25. Solid45 element is used to model the tower, the three-dimensional soil layer as well as the piles.

Linear elastic material behavior is assumed for the tower, pile, and soil. The elastic modulus of the tower and the pile are taken as  $3.58 \times 10^9 \text{ Pa}$  and  $3.45 \times 10^9 \text{ Pa}$ , respectively. The Poisson's ratio and the density of concrete are 0.15 and  $26 \text{ KN/m}^3$ , respectively, for both tower and pile. Elastic continuum approach is adopted for modeling the soil. The size of the soil layer was decided based on the boundary effect. The soil up to four times the width of foundation on sideways is considered in the analysis.

To better understand the physical problem, three alternative soil conditions are examined. For the FE model, the elastic modulus of the top layer soil is set to be infinite (fixed support),  $2.63 \times 10^9 \text{ Pa}$  and  $2.63 \times 10^8 \text{ Pa}$ , respectively. The corresponding results of the three cases are summarized in Table.3.

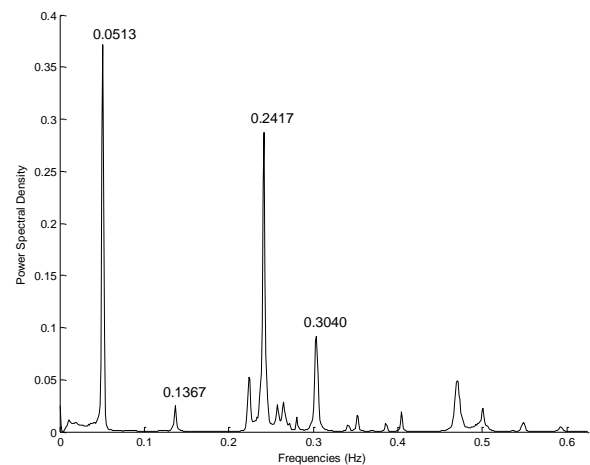


Fig. 24 PSD of the lateral response of the main girder

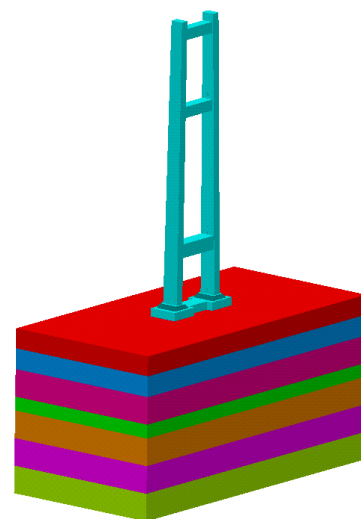


Fig. 25 The 3D FEM of the tower, piles and soil

Table 3 Effects of the soil-structure interaction on the dynamic properties of the tower(Hz)

	Measured (C0)	Soil elastic modulus (N/m <sup>2</sup> )			Relative change (%)			
		Fixed (C1)	2.63e9 (C2)	2.63e8 (C3)	(C1-C0) /C0	(C2-C0) /C0	(C3-C0) /C0	
Longitudinal	L1	0.192	0.198	0.192	0.187	3.1	0	-2.6
	L2	1.080	1.103	1.061	1.016	2.1	-1.8	-5.9
	L3	2.630	2.654	2.560	2.558	0.9	-2.7	-2.7
Lateral	LL1	0.350	0.371	0.359	0.354	6.0	2.6	1.1
	LL2	1.400	1.500	1.468	1.438	7.1	4.9	2.7
Torsional	T1	0.770	0.852	0.807	0.792	10.6	4.8	2.9
	T2	2.130	2.294	2.214	2.135	7.7	3.9	0.2

The effect of pile-soil-structure interaction has a considerable influence on the dynamic characteristics of the tower. Discrepancies in the order of -5.9%~10.6% are observed between the identified and the numerically calculated natural frequencies, highlighting the importance of accurate estimation of pile foundation stiffness. Specifically, for the case of C1, without considering the pile foundation, natural frequencies are obviously higher than the other cases. For the Cases C2 and C3, the calculated frequencies match better with the measured ones.

## 5.2 Initial estimation of the pile foundation stiffness

Although a FE model using solid elements can usually give accurate results, it is time-consuming. Instead, a validated and updated beam model would be more effective in conducting seismic analysis and/or structural health assessment. Along this line, to account for the pile-soil-structure interaction, a lumped parameter foundation model could be used to simulate the pile foundation, as illustrated in Fig. 26. Using this method, the pile foundation system, including piles, soil and rigid pile cap, is modeled by a set of uncoupled springs and dashpots that represent the dynamic impedance function of the foundation (Novak 1974, Damgaard, Andersen *et al.* 2015). The impedance function has a real part and an imaginary part. The real part represents the true stiffness and defines directly the stiffness constant, while the imaginary part describes the out-of-phase component and represents the damping due to energy dissipation in the soil medium. These foundation springs and dashpots are then used as boundary condition for dynamic response analysis of the structure.

The pile foundation stiffness is composed of six uncoupled linear stiffness: longitudinal stiffness  $k_1$ ; lateral stiffness  $k_2$ ; torsional stiffness along the lateral axis  $k_3$ ; torsional stiffness along the longitudinal axis  $k_4$ ; torsional stiffness along vertical axis  $k_5$  and vertical stiffness  $k_6$ .

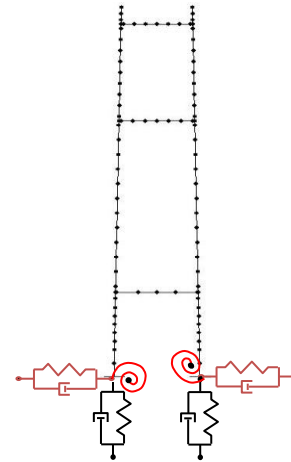


Fig. 26 The beam finite model of the tower with a simplified foundation

The linear dynamic foundation springs and dashpots, in general, are obtained from numerical analysis of pile foundations. The approximate analytical technique developed by Novak (Novak 1974, Novak and Elsharnouby 1983) derives stiffness and damping constants for piles and pile group, with the help of which the initial pile foundation stiffness can be determined. The horizontal, vertical and rocking stiffness of a single pile are respectively calculated as follows

$$k_{xx}^1 = \frac{E_p I}{r^3} f_{x1}, \quad k_{zz}^1 = \frac{E_p A}{r} f_{z1}, \quad k_{\phi\phi}^1 = \frac{E_p I}{r} f_{\phi1} \quad (1)$$

where  $E_p$  is pile Young's modulus;  $r$  is pile radius, and  $A$  is the cross-section area.  $f_{x1}$ ,  $f_{z1}$ ,  $f_{\phi1}$  are dimensionless stiffness parameters, which are based on the ratio of shear wave velocity of the soil to the longitudinal wave velocity of the pile. Thus, the corresponding horizontal, vertical and rocking stiffness of the pile group can be obtained by

$$k_1 = k_2 = \sum_1^{16} k_{xx}^1 \quad (2)$$

$$k_3 = k_4 = \sum_1^8 k_{zz}^1 x_{r1}^2 + \sum_1^8 k_{zz}^1 x_{r2}^2 + \sum_1^{16} k_{\phi\phi}^1 \quad (3)$$

$$k_5 = \sum_1^{16} k_{xx}^1 x_r^2 = \sum_1^8 k_{xx}^1 x_{r1}^2 + \sum_1^8 k_{xx}^1 x_{r2}^2 \quad (4)$$

$$k_6 = \sum_1^{16} k_{zz}^1 \quad (5)$$

For the suspension tower, the corresponding value of above parameters are taken as  $E_p = 3.45 \times 10^4 \text{ N/m}^2$ ,  $r = 1.4 \text{ m}$ ,  $l = 60 \text{ m}$ ,  $l/r \approx 42$ ,  $x_{r1} = 3.14 \text{ m}$ ,  $x_{r2} = 9.41 \text{ m}$ . And from literature (Novak 1974), the parameters  $f_{x1}$ ,  $f_{z1}$ ,  $f_{\phi1}$  are taken as 0.04, 0.05 and 0.450, respectively. Therefore, the initial values of the pile foundation stiffness can be estimated from Eqs. (2)-(5) as:  $k_1 = k_2 = 2.40 \times 10^4 \text{ N/m}$ ,  $k_3 = k_4 = 6.50 \times 10^4 \text{ N} \cdot \text{m}$ ,  $k_5 = 1.20 \times 10^4 \text{ N} \cdot \text{m}$ ,  $k_6 = 1.10 \times 10^4 \text{ N/m}$ .

### 5.3 Probabilistic FE model updating for the pile foundation stiffness

Due to the uncertainties for initial estimation of the pile foundation stiffness, the estimated values are yet to be updated. In this section, the stiffness of the foundation springs as well as the elastic modulus of the tower are identified and updated using correlation analysis, sensitivity analysis and a Bayesian parameter estimation algorithm.

#### 5.3.1 Probabilistic FE model updating formulation

Bayes' theorem is employed to derive the optimal model parameters  $\theta$  given the modal information  $D$  (Beck and Katafygiotis 1998, Beck and Yuen 2004, Sun and Betti 2015). The FE model updating problem would be solved by estimating the distribution of a random parameter with an ensemble of data sets and the prior information. Bayes' theorem is expressed as

$$p(\theta|D, M) = Cp(D|\theta, M)p(\theta|M) \quad (6)$$

where  $p(\theta|D, M)$  is the probability density function (PDF) of the model parameters given modal data  $D$  and model assumptions  $M$ ;  $C$  is a normalizing constant;  $p(\theta|M)$  is the initial ("prior") PDF of model parameters based on engineering and modeling judgment; and  $p(D|\theta, M)$  is the PDF of modal data given model parameters. Here, modeling assumptions  $M$  include those used to derive the probability distributions  $p(\theta|M)$  and  $p(D|\theta, M)$ , as well as the structural modeling assumptions.

Eq. (6) shows how the prior probability of a hypothesis

model represented by  $M(\theta)$  is updated to be a posterior probability of  $p(\theta|D, M)$ . The initial PDF on the model parameters  $\theta$  is assumed to be

$$p(\theta) = (2\pi)^{-\frac{N_\theta}{2}} |S|^{-\frac{1}{2}} \exp\left(-\frac{1}{2}(\theta - \theta_0)^T S^{-1}(\theta - \theta_0)\right) \quad (7)$$

which is a joint Gaussian distribution with mean  $\theta_0 \in \mathbb{R}^{N_\theta}$  and covariance matrix  $S \in \mathbb{R}^{N_\theta \times N_\theta}$ , and  $S$  is a diagonal matrix of variances,  $\sigma_i^2$ .

For the observed frequencies, the model equation is

$$\bar{\omega}_{r,j}^2 = \omega_r^2(\theta) + e_{\bar{\omega}_{r,j}^2}, \quad e_{\bar{\omega}_{r,j}^2} \sim N(0, \varepsilon_r^2) \quad (8)$$

where  $\bar{\omega}_{r,j}$  is the  $r$ -th experimental modal frequency ( $r = 1 \dots N_m$ ,  $j = 1 \dots N_s$ ). The PDF model for the modal frequency error  $\varepsilon_{r,j}$  is a zero mean Gaussian PDF with variance  $\varepsilon_r^2$ .

The PDF for  $\bar{\omega}_{r,j}^2$  is

$$p(\bar{\omega}_{r,j}^2|\theta) = c_2 \exp\left(-\frac{1}{2} \frac{\bar{\omega}_{r,j}^2 - \omega_r^2(\theta)}{\varepsilon_r}\right), \quad (9)$$

$$c_2 = (2\pi)^{-\frac{N_s}{2}} \|C_\omega\|^{-\frac{1}{2}}$$

Thus  $p(\theta/D)$  can be expressed as

$$p(\theta|D) = C \exp\left[-\frac{1}{2} J(\theta)\right] \quad (10)$$

$$\text{with } J(\theta) = (\theta - \theta_0)^T S^{-1}(\theta - \theta_0) + \sum_{r=1}^{N_m} J_r(\theta) \quad (11)$$

$$J_r(\theta) = \sum_{j=1}^{N_s} \left[ \frac{(\bar{\omega}_{r,j}^2 - \omega_r^2(\theta))^2}{\varepsilon_r^2} \right] \quad (12)$$

The optimal parameters  $\theta_\alpha$  can be obtained by maximizing  $p(\theta/D)$ , i.e., by minimizing the  $J(\theta)$ :

$$p(\theta_\alpha|D, M) = \max p(\theta|D, M) = \min J(\theta) \quad (13)$$

The automatic updating procedure is entirely developed in ANSYS, using its optimization tools and probability design module. The pile foundation stiffness and the elastic modulus of tower are uncertain parameters to be identified

$$\theta = [k_1 \quad k_2 \quad k_3 \quad k_4 \quad k_5 \quad k_6 \quad E_T]^T \quad (14)$$

where  $E_T$  is the elastic modulus of the tower.

Table 4. Statistics of the random input variables

No.	Name	Unit	Mean $\theta_0$	Standard Deviation $\sigma_i$	Type	Bounds	
						Lower	Upper
1	$k_1$	N/m	2.40E+10	5.00E+09	Gauss	7.62E+09	4.04E+10
2	$k_2$	N/m	2.40E+10	5.00E+09	Gauss	9.95E+09	4.04E+10
3	$k_3$	N·m/rad	6.50E+12	6.00E+11	Gauss	4.82E+12	8.15E+12
4	$k_4$	N·m/rad	6.50E+12	6.00E+11	Gauss	4.72E+12	8.59E+12
5	$k_5$	N·m/rad	1.20E+12	1.00E+11	Gauss	8.97E+11	1.48E+12
6	$k_6$	N/m	1.10E+11	1.00E+10	Gauss	6.76E+10	1.32E+11
7	$E_T$	N/m <sup>2</sup>	3.70E+010	3.80E+08	Gauss	3.58E+10	3.81E+10

Table 5 Statistical properties of the natural frequencies

Frequency	$\omega_1$	$\omega_2$	$\omega_3$	$\omega_4$	$\omega_5$	$\omega_6$	$\omega_7$	$\omega_8$	$\omega_9$
mean	0.1985	0.3802	0.7397	1.1232	1.5720	2.1047	2.1870	2.6270	2.7753
Std( $\varepsilon_r$ )	0.0011	0.0019	0.0038	0.0066	0.0083	0.0112	0.0141	0.0134	0.0192

Table 6 Linear correlation coefficients between input and output variables

	$k_1$	$k_2$	$k_3$	$k_4$	$k_5$	$k_6$	$E_T$
L1	0.107	-0.082	<b>0.806</b>	0.012	-0.105	-0.068	<b>0.428</b>
LL1	0.025	<b>0.320</b>	-0.071	<b>0.261</b>	-0.006	0.036	<b>0.823</b>
T1	<b>0.444</b>	-0.116	<b>0.423</b>	0.005	0.157	-0.010	<b>0.663</b>

To guarantee the physical significance of the updated parameter values, lower and upper bounds are applied. Random analysis is adopted to find the constraints for the uncertain parameters. Table 4 lists the statistics of parameters  $\theta$ .

During the probabilistic analysis, output parameters are iteratively computed as a function of the random input variables, which are generated using Monte Carlo simulation. Table 5 presents the statistical properties of the natural frequencies calculated by the probabilistic analysis.

### 5.3.2 Sensitivity analysis

The influence of random input variables  $\theta$  on individual output parameters  $\omega_r$ , known as "sensitivity", are studied based on correlation coefficients between all random input variables and specified random output parameters. For illustration, Table 6 tabulates the linear correlation coefficients between input variables and three output frequencies (L1, LL1 and T1). It can be seen from Table 6 that: the 1<sup>st</sup> longitudinal mode frequency L1 is more sensitive to the torsional stiffness along lateral axis  $k_3$  and the tower elastic modulus  $E_T$ ; the 1<sup>st</sup> lateral mode frequency LL1 is more sensitive to the lateral stiffness  $k_2$ , the torsional stiffness along longitudinal axis  $k_4$  and the tower elastic

modulus  $E_T$ ; and the 1<sup>st</sup> torsional mode frequency is more sensitive to longitudinal stiffness  $k_1$ , torsional stiffness along the lateral axis  $k_3$  and the tower elastic modulus  $E_T$ .

Fig. 27 plots the evolution histories of the mean values for output parameters L1 and LL1. The curves indicate that there is 95% level of confidence that the "true" mean values and standard deviations are between the upper and lower bounds.

### 5.3.3 Updated results of the pile foundation stiffness

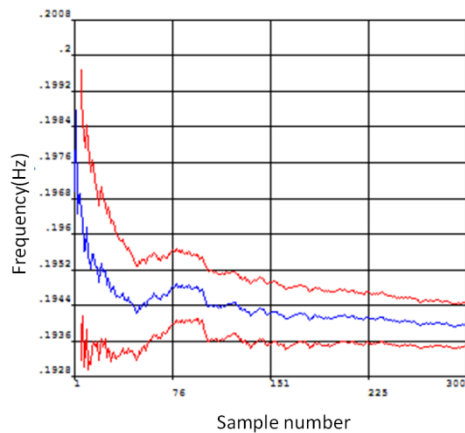
The optimization procedure involves three types of variables: design variables  $\theta$ , state variables  $\omega_r$  and the objective function. In this study, the optimal function is formulated according to the aforementioned Bayesian theorem and given by

$$\min J(\theta) = \min \left\{ (\theta - \theta_0)^T S^{-1} (\theta - \theta_0) + \sum_{r=1}^{N_m} \left[ \frac{(\hat{\omega}_r^2 - \omega_r^2(\theta))}{\varepsilon_r^2} \right] \right\} \quad (15)$$

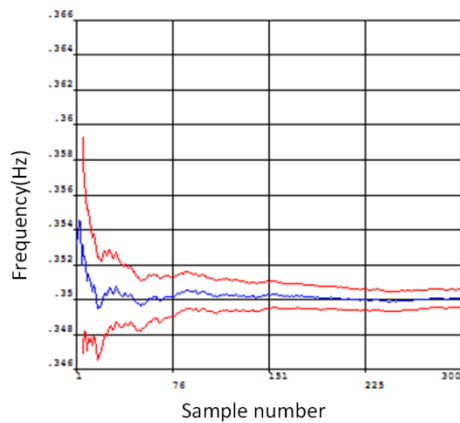
The initially estimated and identified values of the pile stiffness are tabulated in Table 7. It can be seen that the identified parameters  $k_1, k_3, k_4, k_5$ , and  $E_T$  are smaller than the initial ones, while  $k_2$  is larger than its initially estimated value.

Table 7 The initial value and the identified value of the random parameters

Random parameters	$k_1$	$k_2$	$k_3$	$k_4$	$k_5$	$k_6$	$E_T$
Initial value	2.40E+10	2.40E+10	6.50E+12	6.50E+12	1.20E+12	1.10E+11	3.70E+010
Identified value	1.25E+10	4.02E+10	5.08E+12	5.57E+12	1.06E+12	1.06E+11	3.60E+010



(a) L1 mode



(b) LL1 mode

Fig. 27 Mean value history for output parameters L1 and LL1

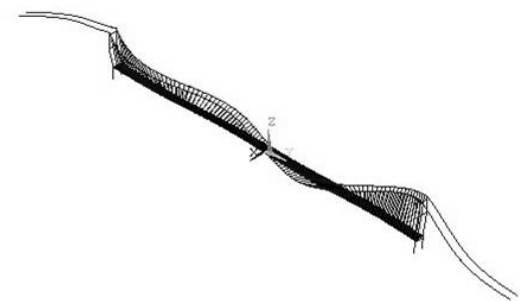
#### 5.4 Finite element modeling of the tower-cable system

Finite element model analysis can help distinguish pure vibrational modes of the suspension tower from coupled vibrations of the tower-cable system, assuming that the FE model can accurately predict structural dynamics.

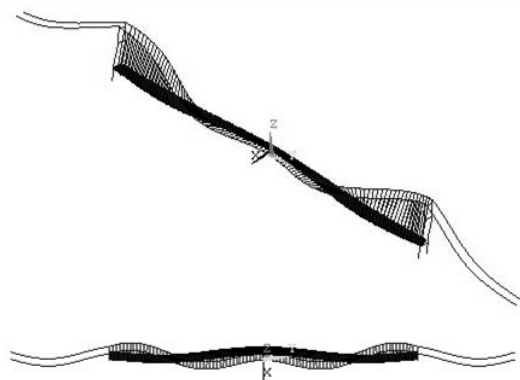
A 3D FE model of RYSB was developed using the commercial ANSYS software. The cables are modeled by tension-only truss elements (LINK10 element), and the pre-tensions of the cables are applied by the initial strains. The towers are modeled using elastic beam elements (BEAM4 element). The steel girder is modeled by shell elements (SHELL63 element). The updated pile foundation stiffness in Section 5.3 is adopted to account for the effect of the pile-soil-structure interaction.

Static analysis is firstly carried out to achieve the deformed equilibrium configuration of the bridge subjected to dead loads, in which the structural members are pre-stressed. Then the dynamic analysis is performed using the Block Lanczos method. The first 30 frequencies and mode shapes from the FE model are summarized in Table 8, and compared with those identified from the ambient vibrations by the SHM system, which shows very good agreements.

As shown in Table 8, vibrations of the suspension bridge comprise of both global vibrational modes and local vibrational modes. The first 6 modes are the girder vibrations, followed by the main-span cable vibrations and side-span cable vibrations. The side-span cable modes exhibit local vibration features. The 25<sup>th</sup> and 26<sup>th</sup> modes are the tower modes, with the corresponding mode shapes plotted in Fig. 28. Due to the coupled vibrations with the cable, there are two closely spaced lateral modes, which are related to the phase of the two towers and the cable. The measured PSDs of the lateral vibration of the tower also confirmed that there are two distinct peaks with frequencies of around 0.34~0.35 Hz.



(a) out-of-phase tower lateral mode and cable vibration



(b) in-phase tower lateral mode and cable vibration

Fig. 28 Calculated lateral modal shapes of the tower-cable system

Table 8 Identified and calculated dynamic properties of the RYSB

Order	Modal shape	Calculated Frequencies ( Hz )	Measured Frequency ( Hz )	Vibration obviously sub-components
1	1rt lateral symmetric bending mode	0.061	0.052~0.059	
2	1rt vertical symmetric bending mode	0.125	0.122	
3	1rt vertical anti-symmetric bending mode	0.143	0.144	
4	1rt lateral anti-symmetric bending mode	0.151	0.137~0.159	girder mode
5	2nd vertical symmetric bending mode	0.170	0.169	
6	2nd vertical anti-symmetric bending mode	0.1900	0.188	
7	out-of-phase sway mode of central span cable	0.202	0.215	
8	out-of-phase sway mode of central span cable	0.208	~	Main-span cable mode
9	in-phase sway mode of central span cable	0.218	0.225	
10	in-phase sway mode of central span cable	0.219		
11	1rt vertical symmetric torsional mode	0.238	0.242	
12	3th vertical symmetric bending mode	0.242	0.240	girder mode
13	in-phase sway mode of side span cable	0.250		
14	in-phase sway mode of side span cable	0.250		
15	out-of-phase sway mode of side span cable	0.256		
16	out-of-phase sway mode of side span cable	0.256	0.232	
17	in-phase in-plane mode of side span cable	0.263	~	side-span cable mode
18	out-of-phase in-plane mode of side span cable	0.263	0.256	
19	in-phase in-plane mode of side span cable	0.269		
20	girder vibration and side span cable vibration	0.273		
21	girder vibration and side span cable vibration	0.275		
22	3th vertical anti-symmetric bending mode	0.292	0.286	
23	1rt vertical anti-symmetric torsional mode	0.293	0.310	girder mode
24	out-of-phase sway mode of central span cable	0.335	NA	central span cable mode
25	Out-of-phase tower lateral mode and cable vibration	0.339	0.342	tower mode
26	in-phase tower lateral mode and cable vibration	0.345	0.354	
27	4th vertical symmetric bending mode	0.347	NA	
28	2nd vertical anti-symmetric torsional mode	0.359	0.371	girder mode
29	out-of-phase sway mode of central span cable	0.365	NA	central span cable mode
30	out-of-phase sway mode of central span cable and in-phase tower lateral vibration	0.381	0.391	tower mode

## 6. Conclusions

Based on a series of field vibration tests conducted on the RYSB during both the construction and operational stages, the dynamic characteristics of the suspension tower of Runyang Suspension Bridge are studied in detail. The conclusions can be summarized as follows:

- (1) Natural frequencies and mode shapes of the freestanding tower are clearly identified from dynamic tests after the tower was erected. It is observed that compared to the identified frequencies, most of the calculated ones from the tower FE model with fixed supports are relatively higher, which probably due to the ignorance of tower-foundation-pile interaction.
- (2) Tower-foundation-pile interaction analysis shows that interaction effect has a considerable influence on the dynamic characteristics of the tower. Discrepancies in the order of -5.9%~10.6% are observed between the identified and numerically calculated natural frequencies when considering different soil elastic modulus in the FE model,

- highlighting the importance of accurate estimation of pile foundation stiffness. In this study, the pile foundation stiffness is successfully identified through a probabilistic FE model updating method.
- (3) The modal parameter evolution of the suspension tower is studied during the construction process. It's found that compared with the identified results from the freestanding tower, the longitudinal and torsional natural frequencies of the tower in the tower-cable system have changed significantly due to the coupled vibrations, while the lateral mode frequencies change slightly. The modal results identified from measurements by the SHM system further confirmed that the vibrations of the bridge subsystems (i.e., the tower, the suspended deck and the main cable) are strongly coupled with one another. To address the modal identification challenges, FE model analyses can be introduced to help distinguish pure vibrational modes of the suspension tower from coupled vibrations of the tower-cable system.

## Acknowledgments

This study was funded by the National Natural Science Foundation of China (Grant Number 51208252) and the National Key Basic Research Program of China (Grant No. 2013CB036300).

## References

- Abdel-Ghaffar, A. and R. Scanlan (1985), "Ambient vibration studies of Golden Gate Bridge: II. Pier-Tower Structure", *J. Eng. – Mech.*, **111**(4), 483-499.
- Beck, J.L. and Katafygiotis, L.S. (1998), "Updating models and their uncertainties. I: Bayesian statistical framework", *J. Eng. Mech. - ASCE*, **124**(4), 455-461.
- Beck, J.L. and Yuen, K.V. (2004), "Model selection using response measurements: Bayesian probabilistic approach", *J. Eng. Mech. - ASCE*, **130**(2), 192-203.
- Brownjohn, J.M., et al. (2005), "Lessons from monitoring the performance of highway bridges", *Struct. Control Health Monit.*, **12**(3-4), 227-244.
- Damgaard, M., et al. (2015), "A probabilistic analysis of the dynamic response of monopile foundations: Soil variability and its consequences", *Probabilist. Eng. Mech.*, **41**, 46-59.
- Deng, Y., et al. (2015), "Investigation of fatigue performance of welded details in long-span steel bridges using long-term monitoring strain data", *Struct. Control Health Monit.*, **22**(11), 1343-1358.
- Feng, D. and Feng, M. (2015), "Model updating of railway bridge using in situ dynamic displacement measurement under trainloads", *J. Bridge Eng.*, 04015019.
- Feng, D., et al. (2015), "A vision-based sensor for noncontact structural displacement measurement", *Sensors*, **15**(7), 16557.
- Feng, D., et al. (2015), "Simultaneous identification of bridge structural parameters and vehicle loads", *Comput. Struct.*, **157**, 76-88.
- Feng, M.Q., et al. (1998), "Identification of a dynamic system using ambient vibration measurements", *J. Appl. Mech. - ASCE*, **65**(4), 1010-1021.
- Gentile, C. and Gallino, N. (2008), "Condition assessment and dynamic system identification of a historic suspension footbridge", *Struct. Control Health Monit.*, **15**(3), 369-388.
- Ko, J.M., et al. (1998), "Modal analysis of suspension bridge deck units in erection stage", *Eng. Struct.*, **20**(12), 1102-1112.
- Li, H., et al. (2011), "Investigation of vortex-induced vibration of a suspension bridge with two separated steel box girders based on field measurements", *Eng. Struct.*, **33**(6), 1894-1907.
- Li, H., et al. (2006), "Structural health monitoring system for the Shandong Binzhou Yellow River Highway Bridge", *Comput. - Aided Civil Infrastruct. Eng.*, **21**(4), 306-317.
- Li, Z.L., Li, A. and Zhang, J. (2010), "Effect of boundary conditions on modal parameters of the Run Yang Suspension Bridge", *Smart Struct. Syst.*, **6**(8), 905-920.
- Ni, Y.Q., et al. (2015), "Investigation of mode identifiability of a cable-stayed bridge: comparison from ambient vibration responses and from typhoon-induced dynamic responses", *Smart Struct. Syst.*, **15**(2), 447-468.
- Novak, M. (1974), "Dynamic stiffness and damping of piles", *Can. Geotech. J.*, **11**(4), 574-598.
- Novak, M. and Elsharnouby, B. (1983), "Stiffness constants of single piles", *J. Geotech. Eng. – ASCE*, **109**(7), 961-974.
- Ren, W., et al. (2004), "Roebing suspension bridge. II: Ambient testing and live-load response", *J. Bridge Eng.*, **9**(2), 119-126.
- Rice, J.A. et al. (2010), "Flexible smart sensor framework for autonomous structural health monitoring", *Smart Struct. Syst.*, **6**(5-6), 423-438.
- Rune, B., et al. (2001), "Modal identification of output-only systems using frequency domain decomposition", *Smart Mater. Struct.*, **10**(3), 441.
- Siringoringo, D.M. and Fujino, Y. (2012), "Observed along-wind vibration of a suspension bridge tower", *J. Wind Eng. Ind. Aerod.*, **103**, 107-121.
- Sun, H. and Betti, R. (2015), "A hybrid optimization algorithm with bayesian inference for probabilistic model updating", *Comput. - Aided Civil Infrastruct. Eng.*, **30**(8), 602-619.
- Sun, H. and Bueyuekoeztuerk, O. (2016), "Probabilistic updating of building models using incomplete modal data", *Mech. Syst. Signal Pr.*, **75**, 27-40.
- Sun, H., et al. (2017), "Bayesian characterization of buildings using seismic interferometry on ambient vibrations", *Mech. Syst. Signal Pr.*, **85**, 468-486.
- Ulusoy, H.S. and Feng, M.Q. (2011), Modal parameter identification of civil engineering structures under operational conditions.
- Van Overschee, P. and De Moor, B. (2012), Subspace identification for linear systems: Theory—Implementation—Applications, Springer Science & Business Media.
- Zhang, J., et al. (2012), "Experimental vibration analysis for structural identification of a long-span suspension bridge", *J. Eng. Mech. – ASCE*, **139**(6), 748-759.

BS